Centrifugal and profile effects on the internal kink mode stability in tokamaks with toroidal plasma flows

C. Wahlberg,[1] I. T. Chapman[2] and J. P. Graves[3]

[1]*Department of Physics and Astronomy, EURATOM/VR Fusion Association, P.O. Box 516, Uppsala University, SE-751 20 Uppsala, Sweden*
[2]*EURATOM/CCFE Fusion Association, Culham Science Centre, Abingdon, Oxfordshire OX14 3DB, United Kingdom*
[3]*Centre de Recherches en Physique des Plasmas, Association EURATOM-Confederation Suisse, EPFL, 1015 Lausanne, Switzerland*

Introduction. It is well established experimentally that the strong toroidal rotation that can be achieved in modern, NBI heated tokamaks (especially in spherical tokamaks) has a favourable effect on the global stability of the plasma, including also modified sawtooth behaviour and internal kink stabilisation [1]. In order to improve the understanding of possible stabilising mechanisms, the present work investigates toroidal flow effects on the ideal $m = n = 1$ internal kink mode in rotating tokamak plasmas both analytically and numerically. The work builds on and extends previous analytical [2] and numerical [3] MHD studies of this instability in rotating plasmas, and by the combination of numerical computation and analytical theory we can identify the properties of toroidal flows that are mainly influencing this instability [4]. In the analytical part, we use a plasma model parametrised such that the centrifugal terms in the plasma equilibrium can be traced through the stability analysis and identified in the final growth rate. The numerical part is based partly on the stability code MISHKA-F [3], and partly on the code CASTOR-FLOW [5] which, in contrast to MISHKA-F, includes the centrifugal effects from the rotation in the plasma equilibrium.

Analytical equilibrium and growth rate. We express the equilibrium profiles of the pressure p, density ρ and the poloidal beta value β_p of the plasma in the form

$$\frac{p(r,\theta)}{p_0(r)} = \frac{\rho(r,\theta)}{\rho_0(r)} = \exp\left[\frac{\sigma_1 \rho \Omega^2 \left(R^2 - R_0^2\right)}{2p}\right], \tag{1a}$$

$$\beta_p = -\frac{2\mu_0 R_0^2 q^2}{B_0^2 r^4} \int_0^r r'^2 \frac{d}{dr'}\left(p_0 + \sigma_2 M^2 p_0\right) dr', \tag{1b}$$

respectively. Here, R and B_0 denote the major radius and the toroidal magnetic field of the plasma (R_0 denotes the major radius of the plasma centre), Ω the rotation frequency and $M = \left(\rho \Omega^2 R_0^2 / 2p\right)^{1/2}$ the sonic Mach number. With the parameters $\sigma_1 = \sigma_2 = 1$ we get a self-

consistent equilibrium, whereas for $\sigma_1 = 0$ the centrifugally induced variation of the density and pressure on the flux surfaces $r = const$ is neglected. Similarly, the part of the Shafranov shift that is caused by the centrifugal force is neglected when $\sigma_2 = 0$.

From the large aspect ratio analysis in [4], the growth rate of the $m = n = 1$ internal kink mode in flowing plasmas is given by $\gamma = \left(\gamma_0^2 - \omega_{GAM\,2}^2\right)^{1/2}$ where

$$\frac{\gamma_0}{\omega_A(0)} = -\frac{\pi\delta\hat{W}}{s_1\sqrt{3F_\rho}}\left(\frac{r_1}{R_0}\right)^2, \quad \omega_{GAM\,2}^2 = \frac{\sigma_1\left[M(r_1)\right]^2\left[\Omega(r_1)\right]^2}{3}\left(1-\frac{1}{\Gamma}\right)+\ldots, \qquad (2a, b)$$

$F_\rho = \rho_0(r_1)/\rho_0(0)$, $\Gamma = 5/3$ is the adiabatic index, $\omega_A^2 = B_0^2/\left(\mu_0\rho_0 R_0^2\right)$ the Alfvén frequency, $s_1 = r_1 q'(r_1)$ the magnetic shear at the radius r_1 where $q = 1$, and $\omega_{GAM\,2}^2$ is the frequency of the geodesic acoustic mode (GAM) induced by the rotation [6]. Furthermore, $\delta\hat{W} = \delta\hat{W}_{Bussac} + \delta\hat{W}_{Rot1} + \delta\hat{W}_{Rot2}$ where $\delta\hat{W}_{Bussac}$ is the usual, normalised Bussac potential energy [7] of the internal kink mode in a static plasma, whereas $\delta\hat{W}_{Rot1}$ and $\delta\hat{W}_{Rot2}$ depend on both the rotation profile and the density profile inside $r = r_1$. For the profiles $\Omega(r) = \Omega(0)\left(1 - r^2/(\varepsilon_\Omega^2 R_0^2)\right)$ and $\rho_0(r) = \rho_0(0)\left(1 - r^2/(\varepsilon_\rho^2 R_0^2)\right)$, the expressions for $\delta\hat{W}_{Rot1}$ and $\delta\hat{W}_{Rot2}$ are given by [2, 4]

$$\delta\hat{W}_{Rot1} = \frac{\hat{\Omega}^2}{2}\left(\frac{2}{\varepsilon_\Omega^2} - \frac{1}{\varepsilon_\rho^2}\right), \quad \delta\hat{W}_{Rot2} = (\sigma_2 - 1)\beta_p\hat{\Omega}^2\left(\frac{2}{\varepsilon_\Omega^2} + \frac{1}{\varepsilon_\rho^2}\right), \qquad (3a, b)$$

where $\hat{\Omega} = \Omega(0)/\omega_A(0)$ (denoted by V_0/V_A in the figures below).

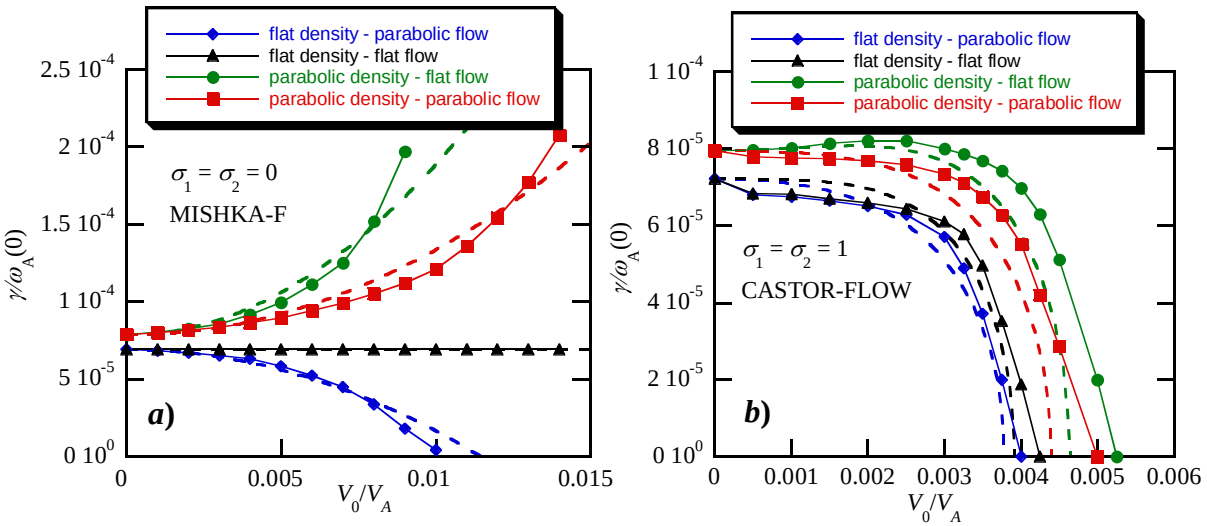

Figure 1. *Growth rate vs rotation velocity at the axis calculated for a non-selfconsistent equilibrium in* ***(a)*** *(σ_1 = σ_2 = 0) and for a selfconsistent equilibrium in* ***(b)*** *(σ_1 = σ_2 = 1). The dashed curves show the analytical predictions and the symbols the numerical results obtained with the two MHD codes indicated. The plasma parameters in both figures are ε_a = 0.1, q_0 = 0.938, r_1/a = 0.3, β_p = 0.3 and β_0 = 0.66 %.*

Analytical and numerical results. Figure 1 shows the growth rate of the $n = 1$ mode in a flowing plasma as a function of the rotation velocity at the axis (normalised with the Alfvén

velocity), calculated both analytically and numerically for different combinations of rotation and density profiles, using an inconsistent equilibrium in Fig. 1a, and a consistent equilibrium in Fig. 1b. The parabolic profiles in the figures correspond to $\varepsilon_\Omega = \varepsilon_\rho = \varepsilon_a = a/R_0 = 0.1$ (a is the plasma minor radius) whereas $\varepsilon_\Omega = \varepsilon_\rho = \infty$ for the flat profiles. Other parameters in the figures are parabolic profiles of q and p_0, with $q_0 = 0.938$, $r_1/a = 0.3$, $\beta_p = 0.3$ and $\beta_0 = 0.66$ %. It is seen that the profiles of density and flow velocity play a crucial role for the rotation-dependence of the growth rate in the inconsistent case. This profile-dependence comes from $\delta\hat{W}_{Rot1} + \delta\hat{W}_{Rot2}$ together with the fact that the (stabilising) GAM frequency in Eq. (2b) vanishes when $\sigma_1 = 0$. With also $\sigma_2 = 0$ in Eq. (3) it is seen that, with $\beta_p < 0.5$, peaking of the rotation profile is stabilising whereas peaking of the density profile is destabilising (for all β_p) in the inconsistent model. In the consistent case $\sigma_1 = \sigma_2 = 1$, on the other hand, the profile dependence (in this case from $\delta\hat{W}_{Rot1}$ only) becomes much weaker due to a strong effect of the finite frequency $\omega^2_{GAM\,2}$ in Eq. (2b), leading to stabilisation already for $V_0/V_A \sim 0.004$-0.005 and, since $\omega^2_{GAM\,2}$ depends on the rotation at $q = 1$ only, with relatively little difference between the different profiles.

With decreasing aspect ratio, the relative importance of $\omega^2_{GAM\,2}$ in comparison with $\delta\hat{W}_{Rot1}$ decreases [4], which leads, for realistic aspect ratios ($\varepsilon_a \sim 0.2$-0.3 and larger), to a significant profile dependence also in the consistent case. This is illustrated schematically in Fig. 2a, which shows the critical rotation required for stabilisation vs ε_a calculated from the analytical theory for a consistent equilibrium with the same parameters as in Fig. 1b.

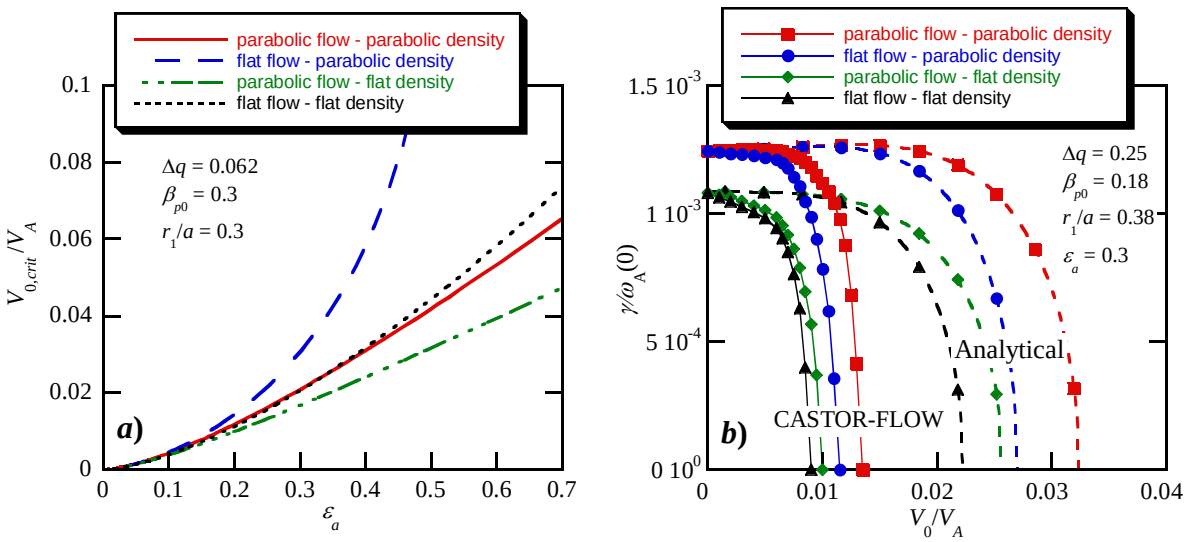

***Figure 2**. **a)** Critical rotation velocity required for stabilisation of the kink mode vs the inverse aspect ratio ε_a shown for four combinations of the profiles of density and rotation for a consistent equilibrium with the parameters indicated. **b)** Growth rate vs rotation velocity at the axis for four different combinations of profiles in a plasma with a large value of Δq. The flow is treated consistently. The dashed curves show the analytical predictions and the symbols the numerical results obtained with CASTOR-FLOW.*

Note that, in contrast to the situation in Fig. 1a, the mode is, for a sufficiently large rotation velocity, stabilised for all profile combinations in Fig. 2a due to the effect of the finite GAM

frequency in the consistent case. Additional examples of profile effects and flow stabilisation, including also realistic MAST equilibria, are given in [4].

With a decreasing q_0, the Bussac part of $\delta\hat{W}$ in Eq. (2a) increases since $\delta\hat{W}_{Bussac} \sim \Delta q$ [7]. Therefore the relative importance of $\delta\hat{W}_{Rot1}$ and the profile dependence included in this term diminishes with a decreasing q_0. Instead, the rotation dependence of β_p in Eq. (1b) becomes more important through the dependence of $\delta\hat{W}_{Bussac}$ on β_p [7]. For parabolic profiles one gets [4] $\beta_p = \beta_{p0} + \sigma_2\hat{\Omega}^2\left(1/\varepsilon_\Omega^2 + 0.5/\varepsilon_\rho^2\right)$. Hence, if the rotation and density both decrease with the minor radius (ε_Ω^2 and $\varepsilon_\rho^2 > 0$) this enhances the "effective" beta value of the plasma, which is destabilising. The equilibrium that is easiest to stabilise in this case has flat profiles of both rotation and density, whereas the combination of parabolic flow and parabolic density is most difficult to stabilise. This is shown in Fig. 2b for a plasma with $q_0 = 0.75$, with qualitative agreement between the analytical theory and the numerical computation. Quantitatively, however, the agreement is not as good as in Fig. 1b due to the larger value of ε_a in Fig. 2b.

Summary. Different mechanisms affecting the stability of the internal kink mode in rotating plasmas have been identified in this work. In the absence of centrifugal effects, the major flow effects on the internal kink instability come from the radial profiles of the plasma density and rotation velocity inside $q = 1$ through $\delta\hat{W}_{Rot1}$ and $\delta\hat{W}_{Rot2}$ in Eq. (3). With the centrifugal effects included, the profile dependence in $\delta\hat{W}_{Rot1}$ is still present, but another stabilising effect arises from the coupling of the internal kink mode to the GAM induced by the plasma rotation, an effect that depends on the rotation at $q = 1$ only. Furthermore, the rotation dependence of β_p in Eq. (1b) leads to a destabilising effect when the flow velocity and plasma density decrease with the plasma radius, and this effect overshadows the profile dependence in $\delta\hat{W}_{Rot1}$ for sufficiently small q_0. While the stabilising GAM coupling dominates when ε_a is small, the importance of both of the profile effects above increases with decreasing aspect ratio.

The authors would like to thank Dr E. Strumberger, Dr H. P. Zehrfeld, Dr C. Konz and their co-workers at IPP Garching for providing us with the CASTOR-FLOW and DIVA codes. This work was partly funded by the United Kingdom Engineering and Physical Sciences Research Council and by the European Communities under the contracts of Association between EURATOM, the Swedish Research Council (VR), UKAEA and the Fonds National Suisse de la Recherche Scientifique. The views and opinions expressed herein do not necessarily reflect those of the European Commission.

References

[1] Lloyd, B. et al., *Nucl. Fusion* **47** S658 (2007); Menard, J. E. et al., *Nucl. Fusion* **45**, 539 (2005).
[2] Waelbroeck, F. L., *Phys. Plasmas* **3**, 1047 (1996); Wahlberg, C. and Bondeson, A. *Phys. Plasmas* **7**, 923 (2000).
[3] Chapman, I. T. et al., *Phys. Plasmas* **13**, 062511 (2006); *Nucl. Fusion* **46**, 1009 (2006).
[4] Wahlberg, C., Chapman, I. T., Graves, J. P., *Phys. Plasmas* **16**, 112512 (2009); Chapman, I. T., Graves, J. P., Wahlberg, C. and the MAST Team, *Nucl. Fusion* **50**, 025018, 2010.
[5] Strumberger, E. et al., *Nucl. Fusion* **45**, 1156 (2005).
[6] Wahlberg, C., *Phys. Rev. Lett.* **101**, 115003 (2008).
[7] Bussac, M. N. et al., *Phys. Rev. Lett.* **35**, 1638 (1975).